Int J Adv Manuf Technol (2016) 87:2459–2470
DOI 10.1007/s00170-016-8660-y

ORIGINAL ARTICLE

# Kinematics modeling and simulating of grinding surface topography considering machining parameters and vibration characteristics

**Xuezhi Wang[1] · Tianbiao Yu[1] · Yuanxing Dai[1] · Ying Shi[1] · Wanshan Wang[1]**

Received: 24 October 2015 / Accepted: 20 March 2016 / Published online: 31 March 2016


**Abstract** Grinding is applied widely in manufacturing of high-precision component. And, pursuing the forming mechanism, together with predicting topography characteristics and roughness of the grinding surface, is becoming more and more important in improving the grinding quality. The grinding surface is formed by the interaction between the grinding wheel and the workpiece. And, its topography is influenced by the grain shape, grinding wheel surface topography, and machining parameters. In this paper, the study started from establishing the topography of wheel surface. And, according to grinding kinematics, the grain trajectory equations were established. By applying the statistical screening methods, the actual cutting depth was determined. Then, the grinding surface topography was formed by simulating. Considering the influence of vibration in actual grinding, the surface topography of the workpiece under forced vibration was studied. The study results showed that the influence of grinding speed was significant for grinding surface topography, mainly in the influence for amplitude and frequency. Finally, the grinding experiments were used to verify the results of the simulation. The obtained experimental results confirmed that the as-proposed method worked efficiently and rapidly in simulating the grinding surface topography and predicting the grinding surface roughness.

✉ Xuezhi Wang
wangxuezhineu@126.com

[1] School of Mechanical Engineering & Automation, Northeastern University, NO. 3-11, Wenhua Road, Heping District, Shenyang 110819, People's Republic of China

**Keywords** Surface topography · Surface roughness · Grinding speed · Vibration

## 1 Introduction

Although grinding is probably one of the oldest manufacturing processes, it still persists as an important component of modern manufacturing [15]. It is due to the fact that it is a finishing process with a low material removal rate, which makes it best suited for producing parts with high precision and high surface quality. And, properties of surface layer created in grinding influence directly the functional properties of the parts such as fatigue strength, abrasive, and corrosion resistance [12]. It has long been recognized that fatigue cracks generally initiate from free surfaces [8]. This is due to the fact that surface layers carry the highest loads and are exposed to environmental effects. Stress concentration, oxidation, and burning out of alloy elements (at high operational temperatures) are the factors acting upon the surface layers that contribute to crack initiation [26]. Surface topography is the microgeometry which is affected by various factors during processing [19]. For grinding, the grinding surface topography is a combination of residual traces, which is formed through the relative movement between the abrasive grains and the workpiece [27]. Surface topography directly affects the abrasion, corrosion, and sealing of parts, which determine its overall work performance and service life. Therefore, in-depth understanding on the as-generated mechanism of grinding surface topography is of great significance in controlling and improving the parts quality during grinding processes.

To do research on grinding precision, uncertainty factors of topography of the grinding wheel must be taken into account, which strongly depends on the randomness of its structure and combinative uncertainty between abrasive grains and binder.

With the advent of high-speed computers, a simulation of the surface interactions becomes feasible, which provides possibility for grinding modeling [13, 14]. In recent years, the progresses are being made on both predicting the surface roughness of grinding surface and modeling topography characteristic for grinding wheel. Zhou and Xi proposed a solution to predict surface roughness considering the random distribution of the grain protrusion heights [27]. Huang et al. [7] analyzed the surface grinding quality of silicon nitride based on the experiments and found that the spindle vibration caused by high wheel speeds could limit the improvement of surface quality. Xie et al. [25] proposed a geometric method to predict the surface topography by utilizing wheel topography data obtained through contact measurement. Pinto et al. [20] combined deterministic and stochastic variables to describe the abrasive layer and simulated the material removal process. Based on Johnson transformation method and linear filter technique, Chen and Tian [4] presented the methodology of machined surface generation in ultra-precision grinding. Assuming the abrasive grains being with three different shapes, referring to the method of trajectory, Liu et al. [17] obtained the topography of grinding surface through simulation. Jiang et al. [9] developed a mathematical method to predict ground surface roughness and topography, based on considering dressing and wearing.

The grinding surface is formed by the interaction between the grinding wheel and the workpiece. And, its topography is influenced by the grain shape, grinding wheel surface topography, and machining parameters. With regard to the generation of the grinding wheel surface by kinematic simulating, the simplest approach is measuring and using the grinding wheel topography directly in the simulation. Usually, the grinding wheel geometry is digitized by two or three-dimensional scanning with conventional stylus instruments, or by optical sensors [23]. Koshy et al. [10] utilized the wheel topography data obtained to simulate three-dimensional structure of the diamond grinding wheel. Aurich et al. [1] modeled the surface topography of electroplated grinding wheel with statistical method by statistically analyzing the scanning electron microscopy (SEM) images of electroplated grinding wheels. Chakrabarti and Paul [3] generated the grinding wheel topography using square pyramidal grits. Gao et al. [21] proposed and established a non-Gaussian mill grinding wheel surface topography model through measuring the topographies of two mill grinding wheels with different grain sizes by using an Olympus confocal scanning laser microscope. Liu et al. [16] generated the grinding pad topography with spherical grains.

In this paper, an efficient new method for simulating the surfaces of grinding wheel and grinding workpieces was proposed. Starting from generating the topography of wheel surface, the abrasive grain trajectory equations were established according to grinding kinematics; after that, the shape of grinding wheel was mapped to the surface of workpiece. Then, the actual grinding depth could be obtained through analyzing and screening the minimum value of the abrasive grain track on every point of the workpiece. In order to get a more realistic topography in simulation, the vibrating factor was taken into account. The simulation results showed that vibration factors must be taken seriously. It would change the actual cutting depth, affect the machining accuracy, and seriously cause devastating damage to grinding surface. Finally, the experimental results after the grinding experiment proved that the above method had a certain guiding significance on grinding surface topography simulation and roughness prediction of the workpiece.

## 2 Topography analysis of grinding wheel surface

### 2.1 Parameters analysis on grinding wheel surface topography

Grinding wheel is a porous body, which is made up of binder, abrasive grains, and pore. In practical processing, the processing quality of workpiece surface is directly affected by topography characteristics of the grinding wheel surface. As a result, the topography of grinding wheel surface is the premise to predict the quality of workpiece surface. The more details of topography characteristics of the grinding wheel are taken into account, the more accurate the prediction could be obtained.

It is generally recognized that the grain protrusion height is defined using Gaussian distribution [21, 24, 27]. And, the grain size is related to the grain number. Based on the previous research, a brief topography analysis of grinding wheel surface is given as follows. In forming the grinding wheel surface topography, grain size and structure number are the two main factors. It is generally believed that the largest size $d_{\max}$, average size $d_{\text{avg}}$ of abrasive grain, mean value $\mu$, and standard deviation $\sigma$ could be given by the following equation [21, 27]:

$$\begin{cases} d_{\max} = 15.2\ G^{-1} \\ d_{\text{avg}} = 68\ G^{-1.4} \\ \mu = d_{\text{avg}} \\ \sigma = \left(d_{\max} - d_{\text{avg}}\right)/3 \end{cases} \tag{1}$$

where $G$ is the grain size. Before analysis, it is necessary to clear the two concepts, which are equivalent diameter and Anderson–Darling test. When the size of longer axis of the measured grain was close to the diameter of a homogeneous sphere, then the diameter of the homogeneous sphere could be seen as the equivalent grain diameter. In order to vividly describe this concept, the schematic diagram of equivalent grain diameter is shown in Fig. 1. In addition, the Anderson–Darling test is a statistical test of whether a given sample of data is drawn from a given probability distribution.

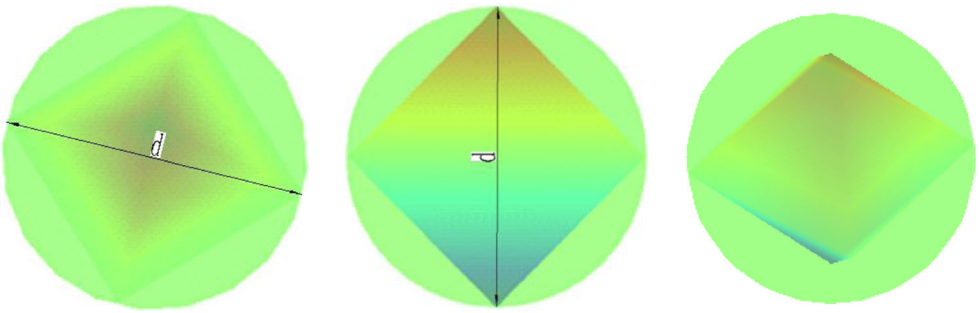


**Fig. 1** The schematic diagram of equivalent grain diameter

(a) Vertical view (b) Front view (c) Oblique view

Based on the principle of seeking truth from facts, the previous results of Eq. (1) were not directly adopted. In order to examine the statistical distribution of equivalent grain diameter, to reveal their dimensional characteristics and to obtain suitable grinding grain size parameters, the grains are measured respectively to evaluate whether they comply with the normal distribution as expected. The equivalent grain diameter is measured as indicated in Fig. 2, and the Anderson–Darling test is used to verify the agreement with the normal distribution of the measured values.

Furthermore, the interval between adjacent two abrasive grains should also be considered. Since the interval has a negative relation with the structure number of the grinding wheel, shown as $S$, the volume percentage $V_g$ (%) of abrasive grains in the grinding wheel can be approximately provided as follows [4, 17]:

$$V_g = 2(32-S)\% \tag{2}$$

Normally, $S$ is the structure number of the grinding wheel, and it varies from 0 to 13 ($0 \le S \le 13$, $S \in N$), where $N$ is a positive integer number set. Hence, $V_g$ (%) could be calculated as 38 to 62.

Based on the as-obtained $V_g$ (%), assuming the distribution of abrasive grains is uniform, the interval between adjacent two abrasive grains can be further calculated.

The relations between $V_g$ (%) and $d_{avg}$ can be represented as

$$\frac{\pi}{6} {d_{avg}}^3 = V_g \Delta^3 \tag{3}$$

where $\Delta$ is the interval between adjacent two abrasive grains. Referring to Eq. (2), and Eq. (3), $\Delta$ can be determined as

$$\Delta = 2.0274\mu \sqrt[3]{\frac{\pi}{32-S}} \tag{4}$$

### 2.2 Modeling on grinding wheel surface topography

For grinding wheel, the topographic characteristic of grains is also important as the dimension parameters and structure parameters. Because the abrasive grain shape has strong randomness, the spherical grain was widely accepted by most scholars [5, 6, 10, 11, 22, 24]. In order to ensure the correctness, the spherical grain shape was not blindly adopted. As this consideration, after the failure of the grinding wheel, one

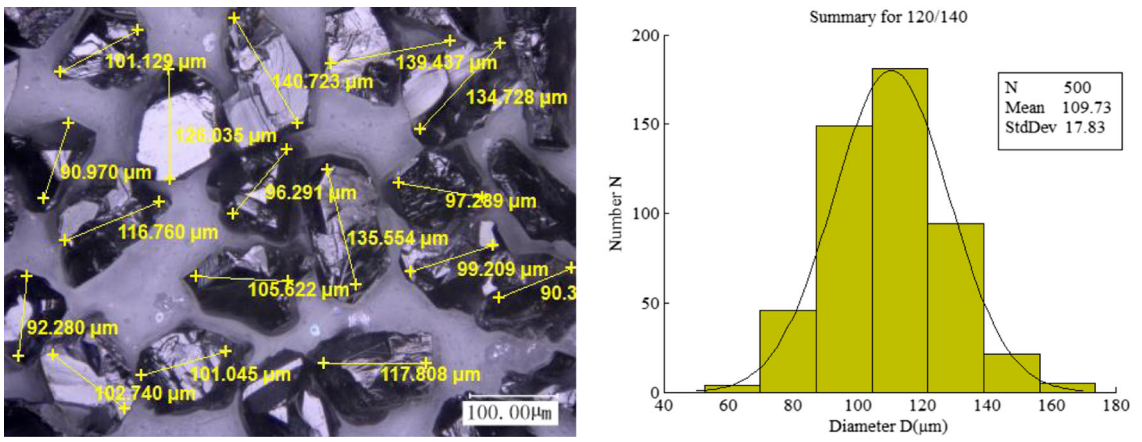


(a) CBN abrasive grains (b) The dimension distribution of grain diameter

**Fig. 2** The analysis of the equivalent grain diameter

of the crack surfaces was taken to the SEM. The surface topography of grinding wheel was observed by scanning electron microscope, and the result is shown in Fig. 3.

In Fig. 3, the surface of grinding wheel was clearly revealed. The distribution of grains is relatively uniform, and most grains are irregular polyhedron. The sharp corners and ridge of grains are very bright. In building the digital grinding wheel surface, the virtual grinding wheel surface should be close to the actual grinding wheel surface as far as possible. In addition, the feasibility also should be considered. Therefore, the shape of the grain was simplified into octahedron in the process of modeling.

Through the above analysis, the model of the whole surface of grinding wheel could be approximately established through five steps. And, the details are shown in Fig. 4. It is worth pointing out that the octahedral cells can be established by two parameters, which are $\mu$ and $\sigma$. First, the octahedral cells with random heights (equivalent grain diameters) were generated by using the two parameters. The distribution of the grain protrusion heights (octahedral cells' heights) is described by a normal distribution with the mean value and standard deviation determined by Anderson–Darling test, and their values are respectively 109.73 and 17.83 μm. Second, by using the uniform point method, the surface of octahedral grains uniform distribution was established. And, it needs to be pointed out that the interval between the adjacent two abrasive grains is the key parameter. Its average value $\Delta$ can be calculated by Eq. (4). Third, the random heights surface of vitrified bond was generated. In theory, in the grinding process, only abrasive grains play the grinding role. So, in this paper, the establishing of the surface of vitrified bond makes the established surface of grinding wheel closer to the actual surface of grinding wheel. Then, the partial grinding wheel's surface was generated by coupling the vitrified bond's surface and the uniform distribution abrasive grains. At last, the whole surface of grinding wheel could be obtained through extending the partial surface of the grinding wheel. It needs to be pointed out that the surface topography of the grinding wheel is not only related to the shapes of abrasive grains but also related to the structure number $G$, the grain size $S$, and the diameter of the grinding wheel.

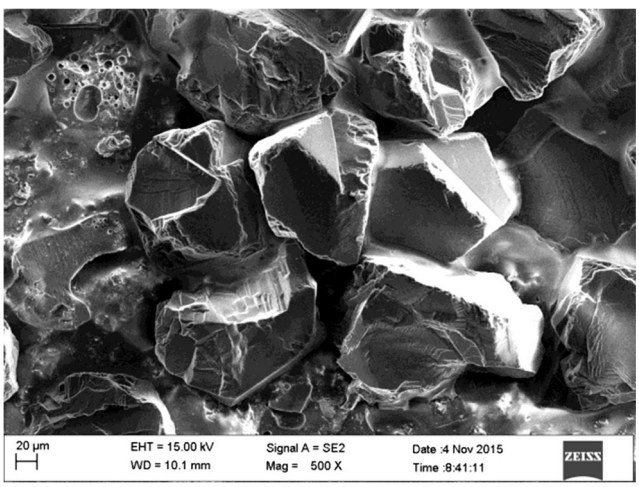


**Fig. 3** The surface topography of grinding wheel

## 3 Topography analysis of workpiece surface

### 3.1 Building simulation model

As there are a lot of factors affecting surface quality of the workpiece, plane grinding process is complex. In order to facilitate the simulation and calculation, the hypotheses here are adopted as follows:

1. The effects of sliding and plowing during the grinding process are not taken into account.
2. There is no vibration during the grinding process.

To simulate the grinding wheel–workpiece interaction, a Cartesian coordinate system of abrasive grain movement was established, and the result is shown in Fig. 5, where the $x$-direction is the horizontal direction (the feed direction of the workpiece), the $y$-direction is along the width of the grinding wheel, and the $z$-direction is the vertical direction (the direction of cutting depth).

The grinding trajectory could be represented as follows [17]:

$$\begin{cases} x_{i,j}(t) = -v_w t + r_{i,j}\sin(\omega - \theta) \\ y_{i,j}(t) = y_{i,j} \\ z_{i,j}(t) = r_{i,j}\cos(\omega t - \theta) \end{cases}, \quad 0 \le t \le t_{\max} \tag{8}$$

where $x_{i,j}(t)$, $y_{i,j}(t)$, and $z_{i,j}(t)$ are respectively the coordinates of the $i,j-$th abrasive grain relative to the workpiece surface at $t$ moment, $v_w$ is the feed rate of workpiece, $r_{i,j}$ is the actual cutting motion radius of the $i,j-$th abrasive grain, $\omega$ is the angular velocity of grinding wheel, and $t_{\max}$ is the maximum cutting time. The subscripts $i$ and $j$ are the serial number of abrasive grains in the direction of circumferential and axial, respectively. Furthermore, $r_{i,j}$ and $\omega$ could be given by $r_{i,j} = r - g_{\max} + g_{i,j}$ and $\omega = v_s/r$, where $r$ is the radius of grinding wheel, $g_{i,j}$ is the protrusion height of abrasive, and $v_s$ is the grinding speed.

During grinding process, only a small number of the abrasive grains on the grinding wheel will contact the workpiece surface. The grinding schematic is shown as Fig. 6.

In the grinding process, when the abrasive grain movement was below the surface, they began to participate in cutting. Such as in Fig. 6a, it clearly reveals the positional relation between the grinding wheel and the workpiece. Prominent

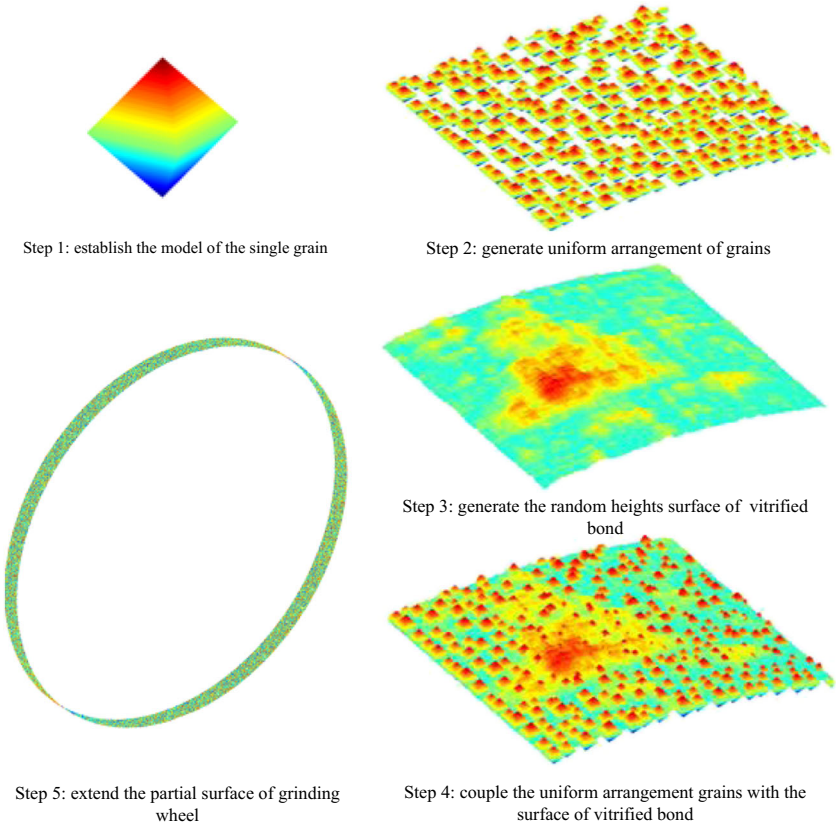


**Fig. 4** The generating process of the whole grinding wheel's surface

grains on relative height will leave the trace of carving on the workpiece surface, as shown in Fig. 6b. In order to further explore the regularity of grinding surface topography, the grinding trajectory model of single grain is established, as shown in Fig. 6c.

The similar approach has been used to perform simulation of the conventional grinding process where no ultrasonic vibration is applied to the workpiece. The workpiece is divided up into grids. Each grid point $g_{i,j}$ is defined in the global coordinate system o'−xyz, with the subscripts $i$ and $j$ corresponding to the positions of the workpiece surface in the $x$ and $y$ direction, respectively. When the abrasive grain moves to the lowest point, its $z$ value in o′- xyz coordinate system can be represented as

$$Z_{i,j,0} = -g_{i,j} + g_{\max} \tag{9}$$

In simulating of grinding surface topography, the workpiece surface is divided into several small elements, and the interval between the adjacent two elements is $\Delta$. The $z$ value of point B in o′-xyz coordinate system can be expressed as

$$Z_{i,j,k} = Z_{i,j,0} + l_{AB}\sin\beta \tag{10}$$

In geometry, the corresponding inscribed angle and central angle has the following relationship:

$$\beta = \frac{\alpha}{2} = \frac{k\Delta}{2r} \tag{11}$$

On account of $a_p << r$, the expression $l_{AB} = l_{CB} = l_{AB}$ could be obtained. In addition, when $\beta$ is very small, $\sin\beta \approx \beta$. So Eq. (9) can be expressed as

$$Z_{i,j,k} = -g_{i,j} + g_{\max} + \frac{k^2\Delta^2}{2r} \tag{12}$$

During grinding progress, each abrasive grain was mapped onto the spatial coordinate, and the time-dependent trajectories could then be obtained by numerically solving Eq. (8). As it is possible that several abrasive grains may pass over the

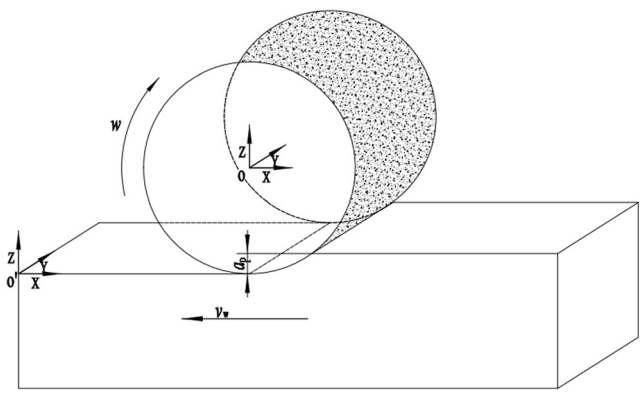


**Fig. 5** Coordinate system of abrasive grain movement

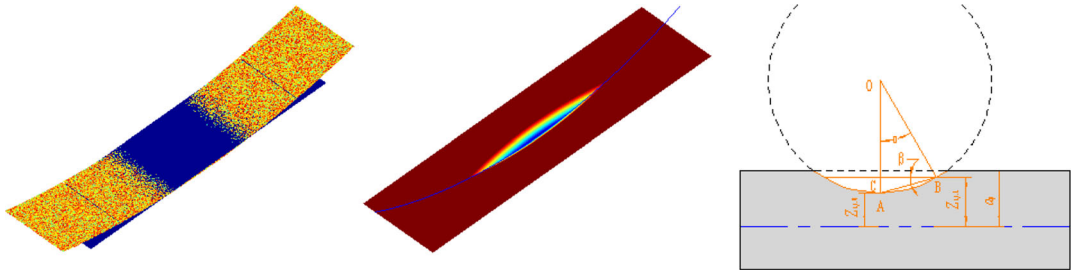


(a) Grinding trajectory of wheel (b) Cutting topography of single-grain (c) Grinding trajectory of single-grain

**Fig. 6** Grinding schematic

same $y$-location, there are generally several solutions for the $z$-coordinate. However, it is only the minimum $z$-coordinate that contributes to generate the eventually finished workpiece surface. So the surface topography of the workpiece can be described by Eq. (14).

In simulating workpiece surface topography, the distances of adjacent units of workpiece surface are equidistant, and the value is $\Delta$. So a conclusion could be obtained, that is, when the workpiece is fed a unit of distance, the grinding wheel would turn a longer distance, and the ratio could be expressed as

$$u = \mathrm{fix}\left(\frac{v_\mathrm{s}}{v_\mathrm{w}}\right) \tag{14}$$

For in-depth research on grinding surface topography, the grinding process is divided into multiple stages, and the basic time interval is $\Delta t$ ($\Delta t = \Delta / v_\mathrm{w}$). If each stage is independent, processing surface is formed by a circular arc; the mathematical model can be described as

$$\begin{aligned} w_{m,n}^{k} &= \min\left(Z_{\substack{i,n,0\\ i=\mathbf{i}}}\right) + \frac{k^2\Delta^2}{2r} \\ &= \min\left(-g_{\substack{i,n\\ i=\mathbf{i}}}\right) + g_\mathrm{max} + \frac{k^2\Delta^2}{2r}, -K \le k \le K \cap k \subset N \end{aligned} \tag{15}$$

where $\mathbf{i} = \mathrm{mod}\{[u(m-1)+1, u(m-1)+2, \cdots, um], I\}$, and $K = \mathrm{fix}\left(\sqrt{2ra_\mathrm{p}}/\Delta\right)$. $I$ is a single week abrasive grain number, and it can be represented as

$$I = \mathrm{fix}\left(\frac{2\pi r}{\Delta}\right) \tag{16}$$

For a given point $w_{m,n}$ on the workpiece, its coordinate is defined as $(w_{mn}^x, w_{mn}^y, w_{m,n}^z)$, and $w_{m,n}^z$ is obtained by a reverse calculation. In the whole grinding process, grinding wheel rotates periodically and abrasive grains participate in cutting continuously. This is due to the grinding surface being involved in cutting by all grains. Therefore, the final grinding surface topography could be described as follows:

$$\begin{cases} w_{mn}^x = m\Delta \\ w_{mn}^y = n\Delta \\ w_{mn}^z = \min\left(\left[w_{m,n}^k\right]_{k=-K,-(K-1),\cdots-2,-1,0,1,2\cdots(K-1),K}, a_\mathrm{p}\right) \end{cases} \tag{17}$$

### 3.2 Influence of grinding parameters on surface topography

The final surface topography generated on a grinding wheel is influenced and determined by the dressing conditions. The main parameters affecting the grinding process are grinding speed, feed rate, and cutting depth. As is known to all, a higher grinding speed should reduce the individual chip volume as chip thickness was decreased with increasing of the grinding speed in surface grinding. In order to better understand the influence of grinding speed on the activation of the grinding surface topography, a series of simulations were tried by using the example model. And, the structure number, grain size, and wheel's diameter are, respectively, 5, 120, and 200 mm. Based on established surface of the grinding wheel and the motion equations of abrasive grains, the topography of grinding surface was obtained by Matlab simulation as shown in Fig. 7.

Surface topography of the workpiece has a close relationship with the grinding speed and the feed rate. At a constant feed rate, surface roughness value becomes smaller with increasing of grinding speed. In an ideal situation with no interference of other factors, when the ratio between grinding speed and feed rate is large enough, the surface will appear as a smooth peak valley which is like a plane surface. Using the same grinding wheel and ignoring the disturbance of other factors, the roughness value of grinding surface keeps a proportional relationship with grinding speed. With increasing of grinding speed, the roughness value of grinding surface tends to approach the minimum value.

The action of feed rate is similar to the grinding speed, with increasing of feed rate, grinding efficiency is improved significantly, and the number of effective abrasive grains increases

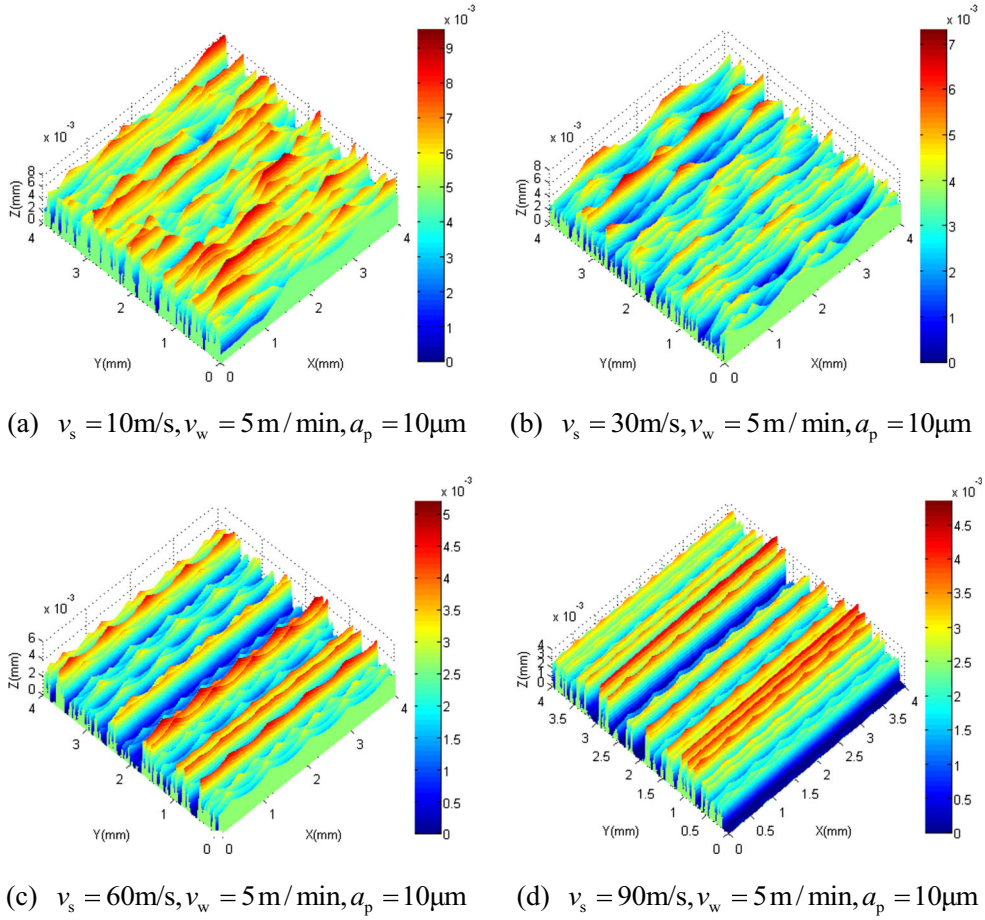


(a) $v_s = 10\text{m/s}, v_w = 5\text{m/min}, a_p = 10\mu\text{m}$ (b) $v_s = 30\text{m/s}, v_w = 5\text{m/min}, a_p = 10\mu\text{m}$

(c) $v_s = 60\text{m/s}, v_w = 5\text{m/min}, a_p = 10\mu\text{m}$ (d) $v_s = 90\text{m/s}, v_w = 5\text{m/min}, a_p = 10\mu\text{m}$

**Fig. 7** The influence of grinding speed on surface topography

at the same time. So more abrasive grains participate in cutting, it makes the grinding surface topography more abundant, and the detailed information is shown in Fig. 8.

Figure 8 shows, with the increasing of feed rate, the grinding track of single-grain growths effectively, and the unevenness of grinding surface increases. For efficiency, the single cycle cutting volume of single grain increases significantly, which will make the grinding force increase in the actual machining. At the same time, the plastic deformation of cutting chips increases, and the tear on the surface also increases.

The cutting depth is the most direct realization of grinding parameters. When the cutting depth is very small, the contact area between the abrasive grain and workpiece is less, the number of effective abrasive grain is less, and the grinding force acting on the workpiece is relatively small. With increasing of the cutting depth, the contact area between the abrasive grain and workpiece gradually increases; the number of effective abrasive grain and the grinding force also increase. So that the surface stress and plastic deformation will increase accordingly. Compressive residual stresses strongly depend on the grinding direction, and significant gradient in the thickness direction. With further increasing of the cutting depth, the portion of material perpendicular to the cutting direction is deformed more plastically than that parallel to the cutting direction by plowing [18]. The specific grinding surface topography under different cutting depths is shown in Fig. 9.

The influence of cutting depth on surface topography was clearly revealed in Fig. 9. When the cutting depth $a_p = 2\mu\text{m}$, there were only some scratches on the grinding surface, and the surface is smooth. This was because the cutting depth was so small that some parts of the surface cannot be continually ground; that is called intermittent grinding. When the cutting depth $a_p = 5\mu\text{m}$, almost the whole surface was cut by abrasive grains, but the height difference of the surface contour was equal to the cutting depth. With further increasing of the cutting depth, the surface roughness increased, and the height difference of surface contour was less than the cutting depth.

### 3.3 Influence of vibration on surface topography

In the actual grinding process, when the spindle rotates at high speed, the vibrations of the grinding wheel will be caused by a slight imbalance due to the imbalance mass. This vibration occurs periodically with rotation of the spindle. Then, the

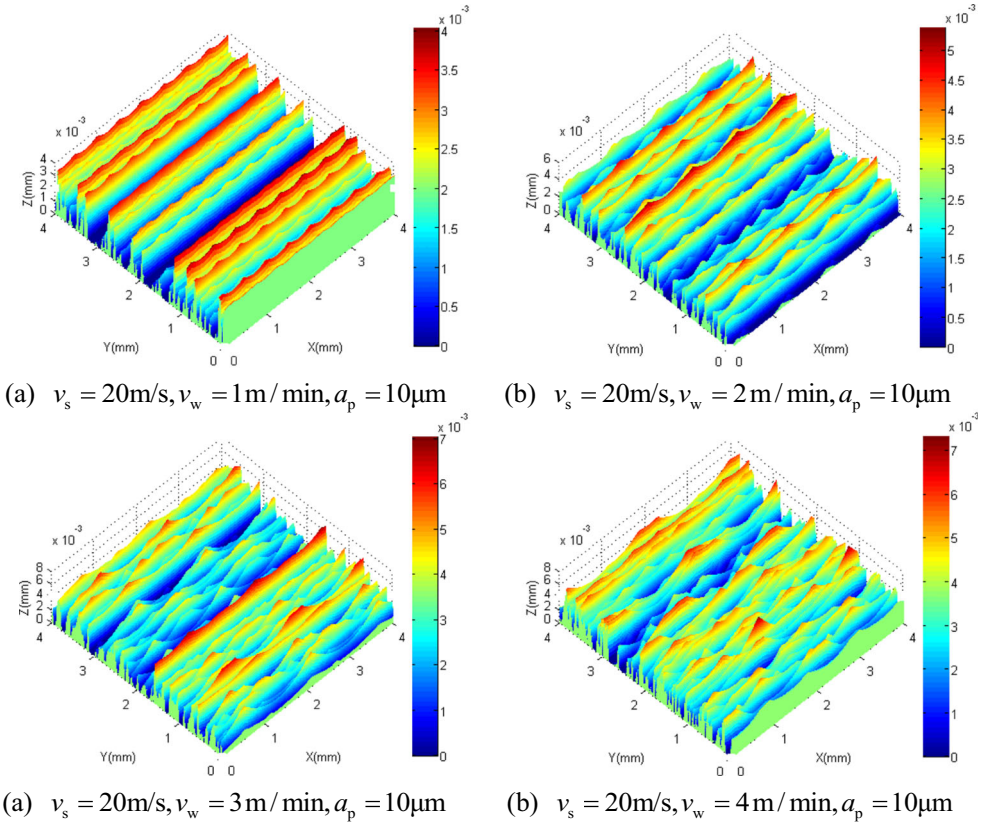


(a) $v_s = 20\text{m/s}, v_w = 1\text{m/min}, a_p = 10\mu\text{m}$ (b) $v_s = 20\text{m/s}, v_w = 2\text{m/min}, a_p = 10\mu\text{m}$

(a) $v_s = 20\text{m/s}, v_w = 3\text{m/min}, a_p = 10\mu\text{m}$ (b) $v_s = 20\text{m/s}, v_w = 4\text{m/min}, a_p = 10\mu\text{m}$

**Fig. 8** The influence of feeding rate on surface topography

abrasive grain trajectories, as well as the surface topography, change correspondingly [2]. The height of the workpiece surface can be expressed as follows:

$$w_{m,n}^{k} = \min_{i=\mathbf{i}} \left( -g_{i,n} + \frac{k^2 \Delta^2}{2r} + A\sin\left( \frac{(u(m-1)+i+k)\omega\Delta t}{u} - \varphi \right) \right) + g_{\max} \tag{18}$$

With generating of the vibration, the grinding wheel fluctuates up and down, which makes the surface in the grinding process become a wavy surface. The vibration equation of the grinding wheel center can be described as

$$M\ddot{\mathbf{z}} + C\mathbf{z} + K\mathbf{z} = me\omega\sin(\omega t) \tag{19}$$

$$\mathbf{z}(t) = A\sin(\omega t - \varphi) \tag{20}$$

where $M$, $K$, and $C$ are, respectively, the total mass, rigidity, and damping of the grinding wheel system, $\omega$ is the rotation angular velocity of the spindle, and $e$ is the eccentricity. Relationships among them could be described by $A = \frac{mer^2}{M\sqrt{\left(1-\lambda^2\right)^2+(2\zeta\lambda)^2}}$, $\varphi = \arctan\frac{2\zeta\lambda}{1-\lambda^2}$, $\zeta = \frac{C}{2\sqrt{MK}}$, $\lambda = \frac{\omega}{\omega_n}$, and $\omega_n = \sqrt{\frac{K}{M}}$, where $A$ is the amplitude, $\varphi$ is the initial phase angle, $\zeta$ is the damping ratio, $\lambda$ is the frequency ratio, and $\omega_n$ is the natural frequency.

For precise grinding machines, the operating speed is far less than the natural angular frequency, which means $\lambda << 1$. Therefore,

$$A = \frac{me}{M\omega_n}\cdot\omega^2 = \alpha\omega^2 \tag{21}$$

It is clearly shown from Eq. (21) that the amplitude of the grinding wheel is proportional to the square of the angular velocity. Assuming $\alpha = 2\times10^{-11}\text{m}\cdot\text{s}^2/\text{rad}^2$ and the workpiece feed rate keeps constant at $v_w = 5\text{m/min}$, surface topography under different grinding speed was calculated and is shown in Fig. 10.

It is shown in Fig. 10 that surface quality is tightly related to the grinding speed. At lower speed, the vibration is not significant, and the surface topography of the workpiece mainly depends on the surface topography of grinding wheel. With increasing of the grinding speed, the influence of vibration becomes increasingly prominent, and the directivity of peak valley appears increasingly obvious on the surface. But, the values of peak valley are lesser.

With increasing of the grinding speed, the amplitude of grinding wheel gradually increases, which makes the actual cutting depth increases significantly. That point is clearly revealed in Fig. 10. Without considering the compressional deformation in the grinding process, the grinding surface topography change is not very obvious, and the characteristic is

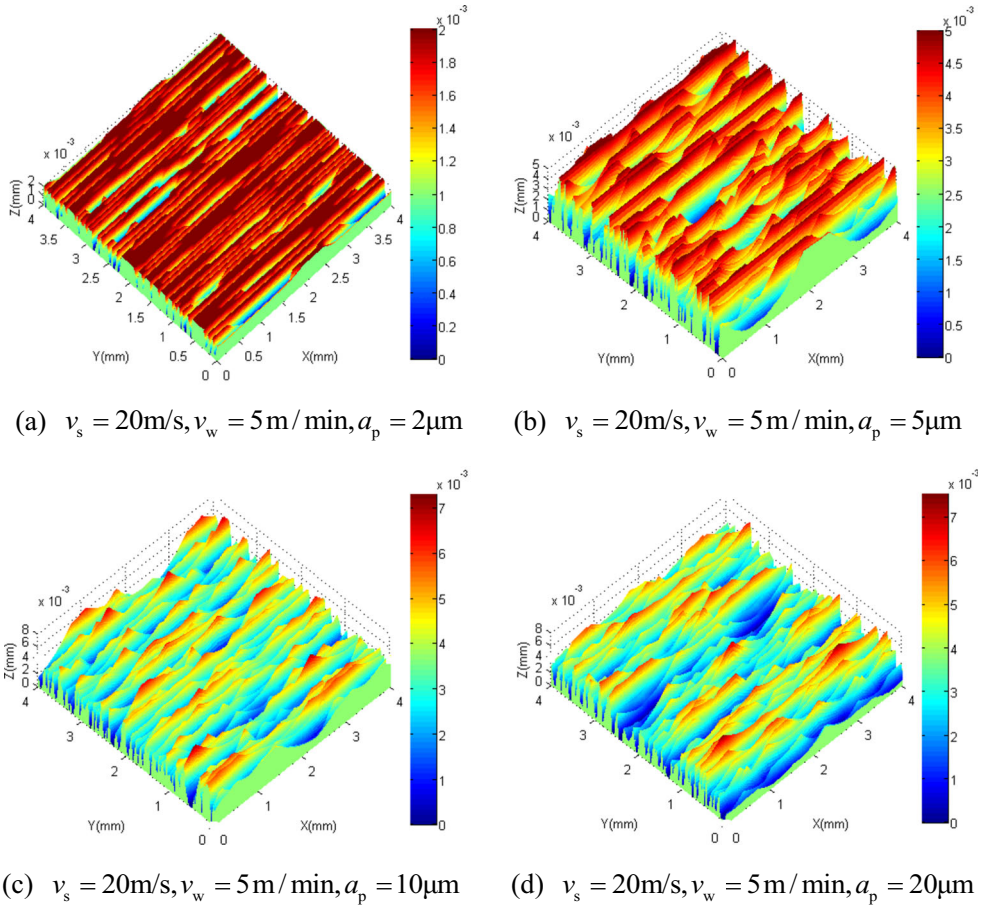


(a) $v_s = 20\text{m/s}, v_w = 5\text{m/min}, a_p = 2\mu\text{m}$ (b) $v_s = 20\text{m/s}, v_w = 5\text{m/min}, a_p = 5\mu\text{m}$

(c) $v_s = 20\text{m/s}, v_w = 5\text{m/min}, a_p = 10\mu\text{m}$ (d) $v_s = 20\text{m/s}, v_w = 5\text{m/min}, a_p = 20\mu\text{m}$

**Fig. 9** The influence of grinding depth on surface topography

different from no vibration machining. In addition, the vibration must be taken into account; otherwise, it is difficult to guarantee the dimensional precision in grinding process. Due to the large cutting depth, the excessive extrusion and tear are out of control.

## 4 Results and discussion

The grinding experiments were carried out on a multi-function grinder (Shenyang Machine Tool (Group) Co., Ltd., M7150), and the grinding wheel used for the experimentation was a medium-grade CBN grinding wheel with a grain size number of 120. The experimental purpose is to study the friction interactions. The maximum running on the wheel was checked and found to be less than 1.5 m. The job specimen, 60 mm long, 25 mm deep, and 20 mm wide, was held in a specially designed fixture. Experimental conditions are specified in Table 1. The grinding surface for all the grinding parameters was studied under a super depth of field three-dimensional display system (VHX-1000E).

The grinding material was titanium alloy Ti-6Al-4V, and the machining tool was CBN grinding wheel. During experiments, the cutting depth $a_p$, the grinding speed $v_s$, and feed rate $v_w$ were considered. The workpiece surface change under the microscope is shown in Fig. 11. In a small cutting depth, the cutting force and the normal force are smaller, and it is easy to form the cutting. With increasing of the cutting depth, the cutting force increases continuously, and the elastic deformation of cutting increases accordingly. Cutting under large cutting, cutting will be sticky on the surface of grinding wheel in different degrees and may even clog pores. And then, tear will appear on the workpiece's surface. This point is revealed clearly in Fig. 11a–c.

Under the condition of the cutting depth unchanged, the increasing of grinding speed is helpful for improving the grinding surface quality. With increasing of the grinding speed, the number of effective grinding increased in per unit time and per unit area. In addition, the plastic deformation could be reduced effectively at high grinding speed, and the material adhesion could be also reduced. The details are shown in Fig. 11d–f.

In addition, with increasing of the feed rate, the grinding efficiency is obviously improved, but the workpiece surface quality becomes lower, and the detailed results are shown in Fig. 11h, i.

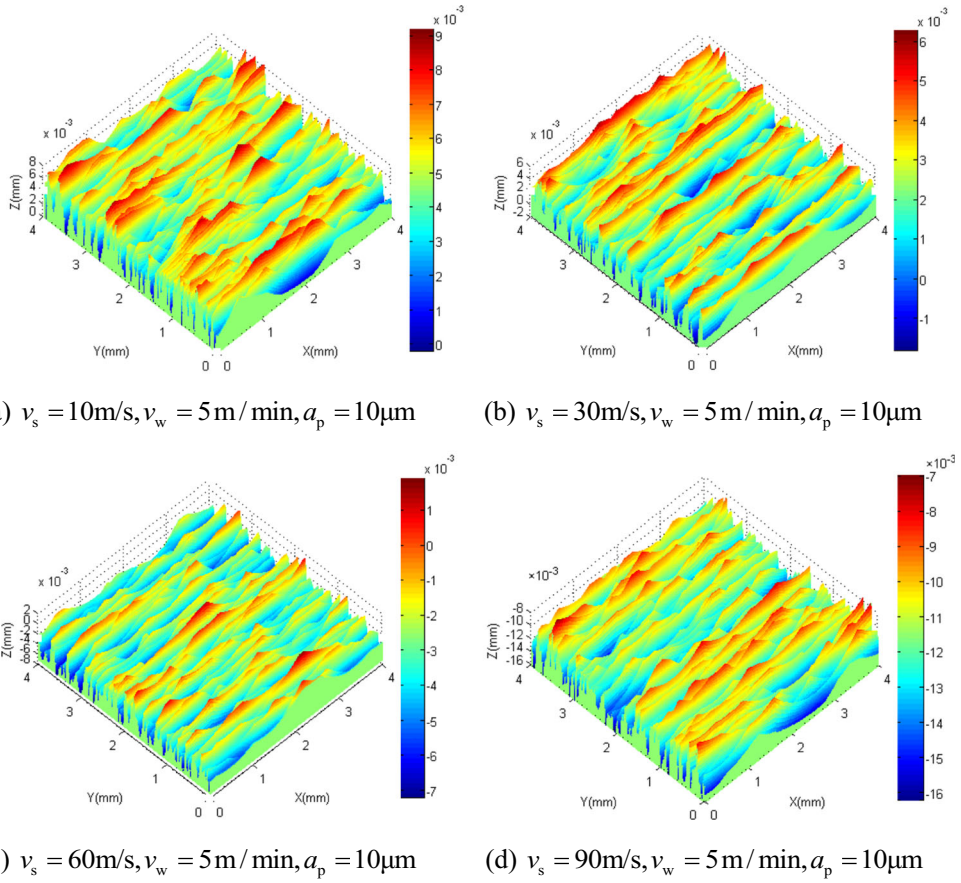


**Fig. 10** Surface topography considering vibration

(a) $v_s = 10\text{m/s}, v_w = 5\text{m/min}, a_p = 10\mu\text{m}$ (b) $v_s = 30\text{m/s}, v_w = 5\text{m/min}, a_p = 10\mu\text{m}$

(c) $v_s = 60\text{m/s}, v_w = 5\text{m/min}, a_p = 10\mu\text{m}$ (d) $v_s = 90\text{m/s}, v_w = 5\text{m/min}, a_p = 10\mu\text{m}$

Grinding topography simulations were realized by using profile modeling method. But, the scratch and tear could not be simulated by using this method. The grinding simulation method is more suitable for high-speed small depth grinding, and the plastic of the grinding material should not be dominant.

To further verify the reliability of the proposed simulation model, a series of grinding experiments were designed. With a constant cutting depth $a_p = 10$ μm, by changing the grinding speed and feed rate, the surface roughness values were obtained and are shown in Fig. 12. Only small errors were found between simulation results and experimental results, and the experimental results were all slightly higher than the simulation results.

**Table 1** The details of grinding conditions

| Grinding mode | Plunge surface grinding, down cut |
|---|---|
| Grinding wheel | P 200 × 10 × 32 CBN 120 VJ50 |
| State of grinding wheel | Fresh (dressing by diamond roller) |
| Workpiece | Titanium alloy Ti-6Al-4V 50 × 20 × 25 (mm) |
| Wheel speed | 10, 20, 30 (m/s) |
| Feed rate | 1, 2, 3,4,5 (m/min) |
| Cutting depth | 1, 2, 5, 8, 10, 20, 30,40(μm) |
| Environments | Dry |

The results of simulation and experiment of this paper showed that actual transition point was larger than that derived from the quasi-static condition. During actual grinding process, there are many other factors influencing the surface quality, such as the hardness of grinding wheel, hardness of material, and grinding depth. However, in this report, only the topography of grinding wheel was considered. Therefore, it is important to point out that the as-proposed model is only applicable to small depth grinding. Next, the comparative study was verified under the small depth grinding. The results are shown in Fig. 13.

According to Fig. 13, the values of surface roughness increased with increasing of the cutting depth $a_p$. In the initial phase, the trends of simulation results and experimental results were consistent; only the values of simulation were slightly higher than experimental values. But, with further increasing of the cutting depth, the differences between the simulation results and experimental results increased gradually. The reason was that the undeformed cutting thickness of single abrasive grain increased along with increasing of the cutting depth, and the cutting force also increased, and then the impact force between grinding wheel and workpiece was great, so the value of surface roughness was large. The results further showed

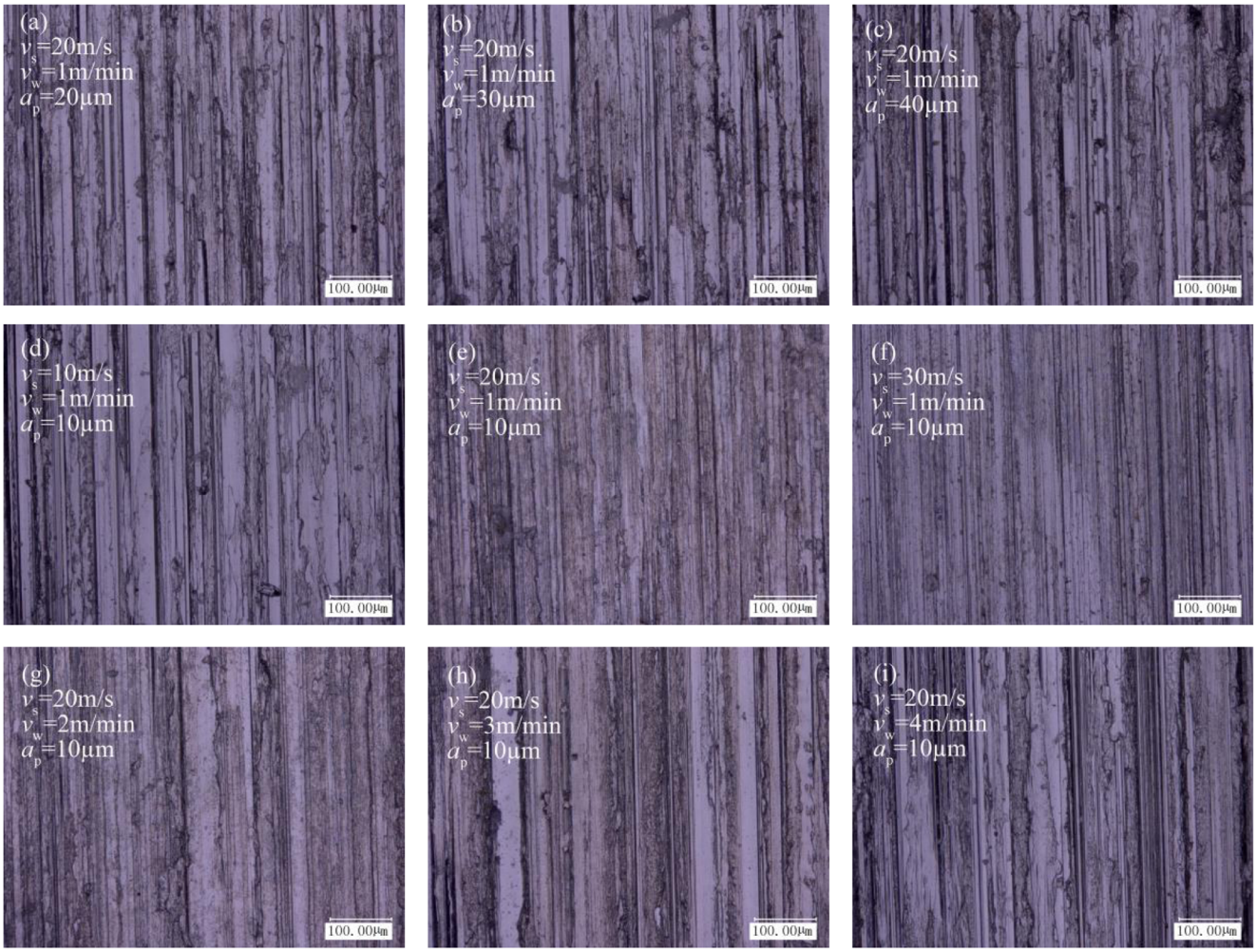


**Fig. 11** The effects of grinding parameters on ground surface topography

that the topography simulation is suitable for small depth grinding. To expand the applicability of the simulation, it is necessary to further consider the influence of other factors on the grinding surface topography.

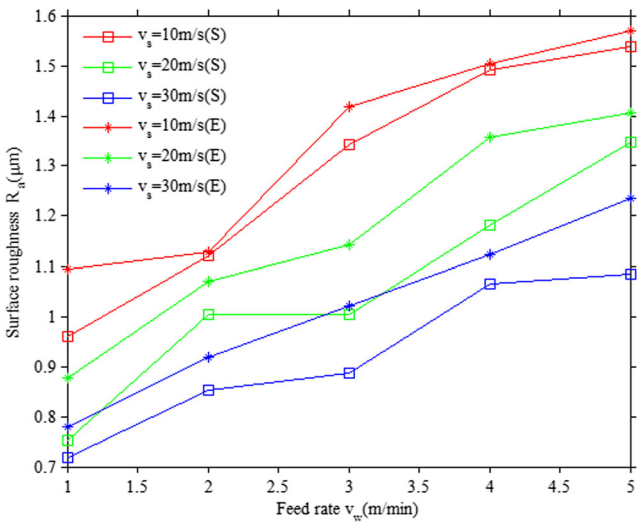


**Fig. 12** The surface roughness under different grinding speeds and different feed rates ($a_p = 10$ μm)

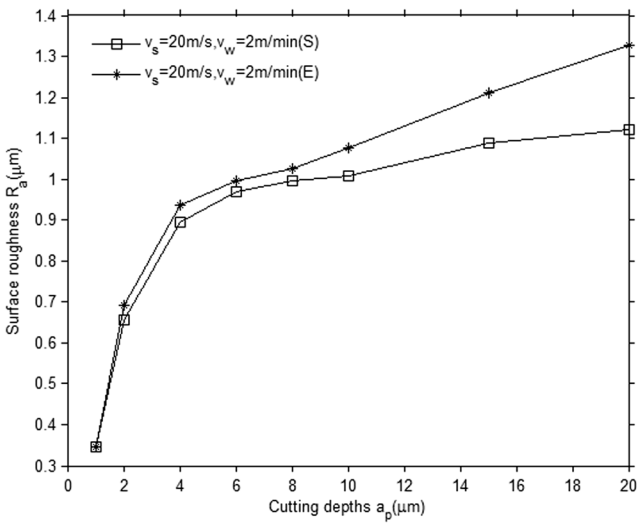


**Fig. 13** The surface roughness under different cutting depths

## 5 Conclusion

In this paper, a fast and feasible simulation method was proposed to visually simulate grinding surface topography and predict grinding surface roughness. The topography characteristics of grinding surface was found to be closely related with the grinding parameters. At small cutting depth, the surface microstructure was improved with increasing of the ratio between grinding speed and feed rate ($v_s/v_w$). As the speed ratio approached a certain value, the directivity of surface peak valley would show up obviously.

The theory of topography analysis was further proved by vibration analysis, where the model is more close to actual grinding process. With constant grinding wheel diameter, amplitude of surface wave depended on the grinding speed, while the frequency depended on the ratio between grinding speed and feed rate. Waviness of the grinding surface could be controlled by adjusting radius of the grinding wheel.

The simulation results showed the surface's characteristics of the grinding wheel and the workpiece. A numerical method was proposed for the kinematic simulation of the grinding process. The method took into consideration the complex nature of the grinding wheel–workpiece interaction by assuming that the attack angle of the abrasive grain would decide the interaction mode. The workpiece surface was updated according to the estimated material removal mode. The agreement between the simulation results and experimental result showed that the method was effective.

**Acknowledgments** This research is supported by the National Nature Science Foundation of China (51275084) and the Key Laboratory Project of Liaoning Province (LZ2015038).

## References

1. Aurich JC, Braun O, Warnecke G (2003) Development of a superabrasive grinding wheel with defined grain structure using kinematic simulation. CIRP Ann Manuf Tech 52(1):275–280
2. Cao Y, Guan J, Li B, Chen X, Yang J (2013) Modeling and simulation of grinding surface topography considering wheel vibration. Int J Adv Manuf Technol 66(5-8):937–945
3. Chakrabarti S, Paul S (2008) Numerical modelling of surface topography in superabrasive grinding. Int J Adv Manuf Technol 39(1-2):29–38
4. Chen D (2010) Modeling and simulation methodology of the machined surface in ultra-precision grinding. J Mech Eng 46(13):186–191 (in Chinese)
5. Chen X, Rowe WB (1996) Analysis and simulation of the grinding process. Part I: generation of the grinding wheel surface. Int J Mach Tools Manuf 36(8):871–882
6. Chen X, Rowe WB, Mills B, Allanson DR (1996) Analysis and simulation of the grinding process. Part III: comparison with experiment. Int J Mach Tools Manuf 36(8):897–906
7. Huang H, Yin L, Zhou L (2003) High speed grinding of silicon nitride with resin bond diamond wheels. J Mater Process Technol 141(3):329–336
8. Javidi A, Rieger U, Eichlseder W (2008) The effect of machining on the surface integrity and fatigue life. Int J Fatigue 30(10-11):2050–2055
9. Jiang JL, Ge PQ, Bi WB, Zhang L, Wang DX, Zhang Y (2013) 2D/3D ground surface topography modeling considering dressing and wear effects in grinding process. Int J Mach Tool Manuf 74(4):29–40
10. Koshy P, Ives LK, Jahanmir S (1999) Simulation of diamond-ground surfaces. Int J Mach Tool Manuf 39(9):1451–1470
11. Koshy P, Jain VK, Lal GK (1997) Stochastic simulation approach to modelling diamond wheel topography. Int J Mach Tool Manuf 37(6):751–761
12. Kruszynski BW, Wojcik R (2001) Residual stress in grinding. J Mater Process Technol 109(3):254–257
13. Law SS, Wu SM (1973) Simulation study of the grinding process. J Manuf Sci Eng 95(4):972–978
14. Law SS, Wu SM, Joglekar AM (1973) On building models for the grinding process. J Manuf Sci Eng 95(4):983–991
15. Li SP, Liang J, Li L, Cao SS, Shu WG, Peng HQ (2003) Study of the ground workpiece surface topography in high-speed precision grinding using a scanning tunneling microscopy. J Mater Process Technol 139(1-3):263–266
16. Liu PF, Lin B, Yan S, Wang B (2015) Numerical simulation and experimental validation of fixed abrasive grinding pad topography. International Journal of Advanced Manufacturing Technology online:1-12
17. Liu YM, Warkentin A, Bauer R, Gong YD (2013) Investigation of different grain shapes and dressing to predict surface roughness in grinding using kinematic simulations. Precis Eng 37(3):758–764
18. Liu X, Zhang B (2002) Effects of grinding process on residual stresses in nanostructured ceramic coatings. J Mater Sci 37(15):3229–3239
19. Nguyen TA, Butler DL (2005) Simulation of precision grinding process, part 1: generation of the grinding wheel surface. Int J Mach Tool Manuf 45(11):1321–1328
20. Pinto FW, Vargas GE, Wegener K (2008) Simulation for optimizing grain pattern on engineered grinding tools. CIRP Ann Manuf Tech 57(1):353–356
21. Qiao G, Dong G, Zhou M (2013) Simulation and assessment of diamond mill grinding wheel topography. Int J Adv Manuf Technol 68(9-12):2085–2093
22. Shiau TN, Chen KH, Wang FC, Chio CT, Hsu WC (2011) The effect of dynamic behavior on surface roughness of ball screw under the grinding force. Int J Adv Manuf Technol 52(5-8):507–520
23. Warnecke G, Zitt U (1998) Kinematic simulation for analyzing and predicting high-performance grinding processes. CIRP Ann Manuf Technol 47(1):265–270
24. Xie Y, Williams JA (1996) The prediction of friction and wear when a soft surface slides against a harder rough surface. Wear 196(1):21–34
25. Xie J, Xu J, Tang Y, Tamaki J (2008) 3D graphical evaluation of micron-scale protrusion topography of diamond grinding wheel. Int J Mach Tool Manuf 48(11):1254–1260
26. Zahouani H, Mezghani S, Vargiolu R, Dursapt M (2008) Identification of manufacturing signature by 2D wavelet decomposition. Wear 264(5-6):480–485
27. Zhou X, Xi F (2002) Modeling and predicting surface roughness of the grinding process. Int J Mach Tool Manuf 42(8):969–977